Report

Cell Reports

MiR-93 Controls Adiposity via Inhibition of *Sirt7* and *Tbx3*

Graphical Abstract

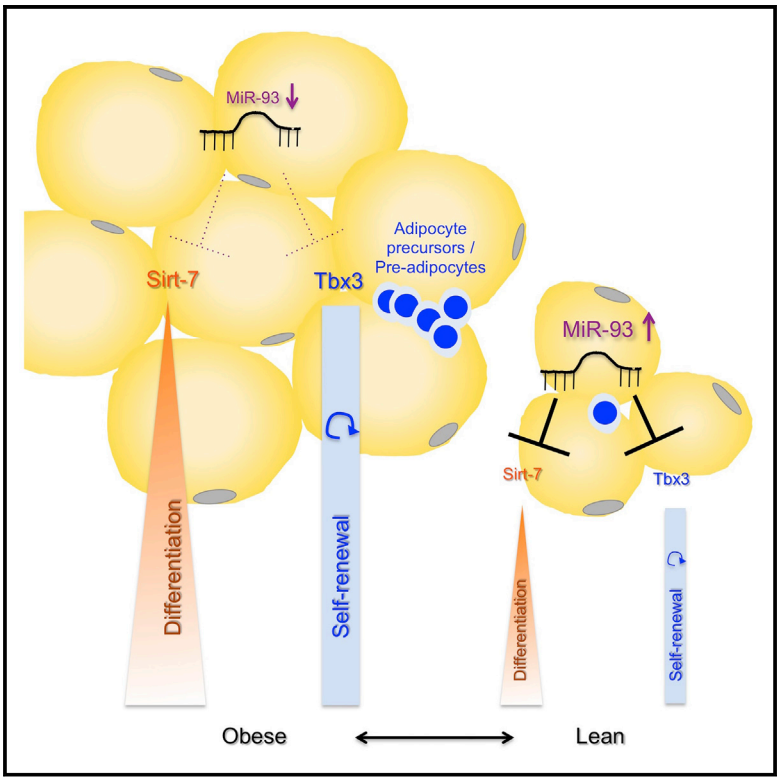

Highlights

- Knockout of the miR-25-93-106b cluster increased fat mass and insulin resistance
- MiR-93 controls *Tbx3* and thereby limits self-renewal of early adipocyte precursors
- MiR-93 further inhibits the metabolic target *Sirt7* and thus in vivo adipogenesis
- (Circulating) miR-93 reduced obesity in miR-25-93-106b KO and *ob/ob* mice

Authors

Michele Cioffi, Mireia Vallespinos-Serrano, Sara M. Trabulo, ..., Anne Moon, Alexandra Aicher, Christopher Heeschen

Correspondence

aicher_a@yahoo.com (A.A.), c.heeschen@qmul.ac.uk (C.H.)

In Brief

Cioffi et al. provide evidence that miRNA-93 suppresses *Tbx3* and *Sirt7*, thereby controlling expansion of adipocyte precursors and inhibiting adipogenesis, respectively.

Cioffi et al., 2015, Cell Reports *12*, 1594–1605
September 8, 2015
http://dx.doi.org/10.1016/j.celrep.2015.08.006

OPEN ACCESS
CellPress

Cell Reports
Report

MiR-93 Controls Adiposity via Inhibition of *Sirt7* and *Tbx3*

Michele Cioffi,[1] Mireia Vallespinos-Serrano,[1] Sara M. Trabulo,[1,10] Pablo Jose Fernandez-Marcos,[2] Ashley N. Firment,[7] Berta N. Vazquez,[8] Catarina R. Vieira,[1] Francesca Mulero,[3] Juan A. Camara,[3] Ultan P. Cronin,[4] Manuel Perez,[5] Joaquim Soriano,[5] Beatriz G. Galvez,[6] Alvaro Castells-Garcia,[1] Verena Haage,[1] Deepak Raj,[10] Diego Megias,[5] Stephan Hahn,[9] Lourdes Serrano,[8] Anne Moon,[7] Alexandra Aicher,[1,10,*] and Christopher Heeschen[1,10,*]

[1]Stem Cells & Cancer Group, Spanish National Cancer Research Centre (CNIO), Madrid 28028, Spain
[2]Tumor Suppression Group, Spanish National Cancer Research Centre (CNIO), Madrid 28028, Spain
[3]Bioimaging, Spanish National Cancer Research Centre (CNIO), Madrid 28028, Spain
[4]Flow Cytometry Unit, Spanish National Cancer Research Centre (CNIO), Madrid 28028, Spain
[5]Confocal Microscopy Unit, Spanish National Cancer Research Centre (CNIO), Madrid 28028, Spain
[6]Spanish National Cardiovascular Research Center (CNIC), Madrid 28028, Spain
[7]Weis Center for Research, Danville, PA 17822, USA
[8]Department of Genetics, Rutgers University, Piscataway, NJ 08854, USA
[9]Department of Molecular Gastrointestinal Oncology, Ruhr-University, Bochum 44801, Germany
[10]Stem Cells in Cancer & Ageing, Barts Cancer Institute, Queen Mary University of London, London EC1M 6BQ, UK
*Correspondence: aicher_a@yahoo.com (A.A.), c.heeschen@qmul.ac.uk (C.H.)
http://dx.doi.org/10.1016/j.celrep.2015.08.006

SUMMARY

Conquering obesity has become a major socio-economic challenge. Here, we show that reduced expression of the *miR-25-93-106b* cluster, or *miR-93* alone, increases fat mass and, subsequently, insulin resistance. Mechanistically, we discovered an intricate interplay between enhanced adipocyte precursor turnover and increased adipogenesis. First, miR-93 controls *Tbx3*, thereby limiting self-renewal in early adipocyte precursors. Second, miR-93 inhibits the metabolic target *Sirt7*, which we identified as a major driver of in vivo adipogenesis via induction of differentiation and maturation of early adipocyte precursors. Using mouse parabiosis, obesity in *mir-25-93-106b*$^{-/-}$ mice could be rescued by restoring levels of circulating miRNA and subsequent inhibition of *Tbx3* and *Sirt7*. Downregulation of *miR-93* also occurred in obese *ob/ob* mice, and this phenocopy of *mir-25-93-106b*$^{-/-}$ was partially reversible with injection of miR-93 mimics. Our data establish miR-93 as a negative regulator of adipogenesis and a potential therapeutic option for obesity and the metabolic syndrome.

INTRODUCTION

Excess visceral adiposity is associated with a variety of metabolic dysfunctions, such as insulin resistance, dyslipidemia, hypertension, and inflammation. In contrast to subcutaneous adipose tissue, enhanced visceral fat mass (evidenced as increased waist circumference) is strongly correlated with higher cardiometabolic risk (Klein et al., 2007). Intra-abdominal visceral fat is biologically distinct from peripheral subcutaneous fat in part by its production of more pro-inflammatory cytokines, which promote insulin resistance, and less adiponectin (Hamdy et al., 2006), which is protective against the development of type 2 diabetes and cardiovascular disease (Nanayakkara et al., 2012). Several microRNAs (miRNAs) previously have been reported to be involved in metabolism and adipogenesis. For example, expression of the *miR-17-92* cluster has been linked to enhanced adipocyte differentiation by negatively regulating tumor suppressor Rb2/p130 (Wang et al., 2008), and both miR-93 and miR-106b have been reported to inhibit brown adipocyte differentiation (Wu et al., 2013). Importantly, *miR-93* expression is decreased during hyperglycemia via repression of *miR-93* promoter activity (Long et al., 2010). Recently, it also was demonstrated that *miR-93* is overexpressed in subcutaneous adipose tissue of young, pre-menopausal, overweight females with insulin resistance: this was mechanistically linked to downregulation of *Glut4* (Chen et al., 2013). However, the role of the miR-25-93-106b cluster, or miR-93 in particular, in the interconnected phenotypes of the metabolic syndrome had not yet been elucidated. To clarify the role of the miR-25-93-106b cluster in adiposity, we set out to identify its targets using *miR-25-93-106b*$^{-/-}$ mice as an in vivo model.

RESULTS

Enhanced Adiposity and Metabolic Syndrome in *mir-25-93-106b*$^{-/-}$ Mice

The *mir-25-93-106b*$^{-/-}$ mice exhibit an increase in the size of visceral fat pads (epigonadal fat; EWAT) on a standard chow diet (Figure 1A). This phenotype was much more pronounced in females, suggesting hormone dependency (Figure S1A). High-fat diet (HFD) further enhanced the phenotype in both

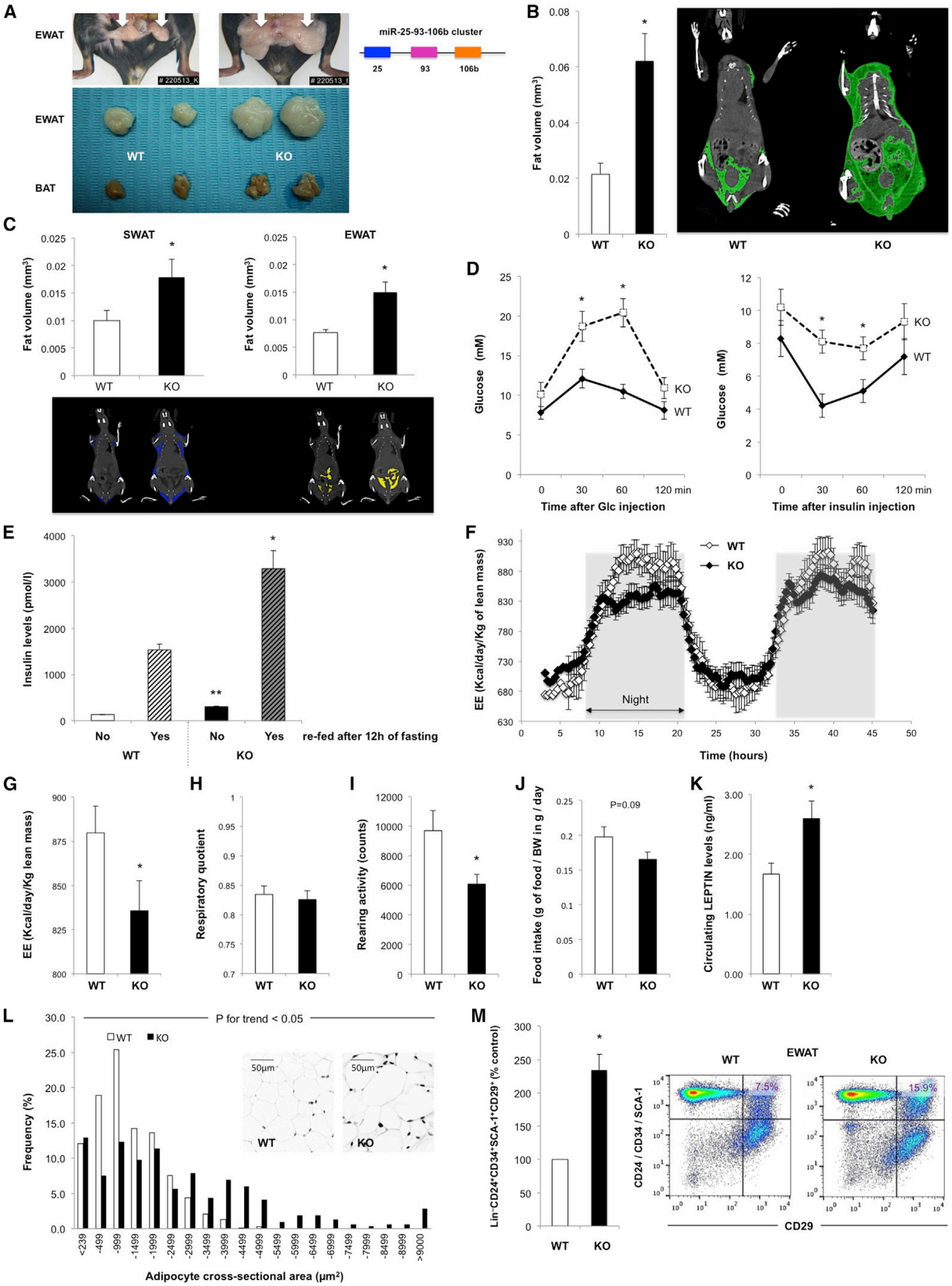

(legend on next page)

male and female mice (Figures S1B and S1C). Females also had increased brown adipose tissue (BAT) (Figure S1D). Visceral fat pad mass of female *mir-25-93-106b*$^{-/-}$ mice started increasing at 8–9 weeks of age (data not shown), which translated into an 18.5% increase in total body weight (BW) by 40 weeks (Figure S1E). This was attributable to both a reduction in lean mass (Figure S1F) and accretion of whole-body, relative fat mass in females (Figure S1G). Differences in males were less prominent (Figure S1H). In addition to enhanced visceral fat, we found increased accumulation of subcutaneous white adipose tissue (SWAT) in females, particularly in the perineal region (Figures 1B and 1C). This excess adiposity resulted in severe glucose intolerance and delayed response to glucose in *mir-25-93-106b*$^{-/-}$ females (Figure 1D, left). In addition, the drop in glucose levels in response to insulin administration was blunted relative to controls, indicating insulin resistance (Figure 1D, right). Consistent with this, endogenous insulin levels after fasting or 2 hr after re-feeding were drastically increased (Figure 1E). Taken together, *mir-25-93-106b*$^{-/-}$ mice are characterized by enhanced adiposity leading to insulin resistance, a key feature of the metabolic syndrome.

Enhanced Adiposity and Adipogenesis in mir-25-93-106b$^{-/-}$ Mice

Energy expenditure (EE) was reduced in *mir-25-93-106b*$^{-/-}$ mice during night hours when mice are most active (Figures 1F and 1G). *Mir-25-93-106*$^{-/-}$ mice had normal respiratory quotients (Figure 1H). However, their reduced rearing activity (Figure 1I) suggests an effect at the level of the CNS. Their food intake was only slightly reduced (Figure 1J), consistent with increased circulating levels of the adipose tissue-derived, anorectic hormone leptin (Figure 1K). This most likely reflects leptin resistance, as is observed in obese individuals when the homeostatic negative feedback loop that normally regulates adipose mass is disrupted (Leyva et al., 1998). The increased size of *mir-25-93-106b*$^{-/-}$ fat pads was attributable to both an increase in the number of large adipocytes (hypertrophic cells) (Figure 1L) and the total number of adipocytes (hyperplasia, Figure S1I). Consistent with this, sorted early adipocyte precursors from *mir-25-93-106b*$^{-/-}$ mice showed enhanced in vitro adipogenesis (Figure S1J). Lipid droplet accumulation was apparent in livers of these mutants, suggestive of liver steatosis, but not in pancreas or kidney (Figures S1K–S1N).

Molecular Characterization of Adipose Tissue in miR-25-93-106b$^{-/-}$ Mice

Infiltration of pro-inflammatory CD11c^{+}CD11b^{+} macrophages into white visceral fat has been linked to insulin resistance (Wentworth et al., 2010), and *mir-25-93-106b*$^{-/-}$ mice had increased infiltration relative to controls (Figure S2A). Concordant with enhanced recruitment of inflammatory cells, stromal cell-derived factor-1 (SDF-1) was augmented, and pro-inflammatory factors interleukin-6 (IL-6) and tumor necrosis factor alpha (TNF-α) were increased (Figure S2B). We also noted enhanced recruitment of bone marrow-derived CD45^{+} fibroblast activation protein (FAP)$^{+}$ stromal cells into visceral fat (Phillips et al., 2004; Figure S2C). Intriguingly, size and number of mesenchymal colonies also were increased in *mir-25-93-106b*$^{-/-}$ mice (Figure S2D).

To elucidate whether differences are already apparent in adipocyte progenitors, we analyzed mesenchymal progenitor cells defined as CD105^{+}SCA-1^{+} cells, and we detected higher numbers of these progenitors in the visceral fat pad of *mir-25-93-106b*$^{-/-}$ mice relative to controls (Figure S2E). Moreover, there were more early adipocyte progenitors (defined as Lin^{-}CD24^{+}CD29^{+}SCA-1^{+}CD34^{+} cells [Berry et al., 2014; Rodeheffer et al., 2008]) in adult visceral adipose tissue of *mir-25-93-106b*$^{-/-}$ mice. This likely contributes to their enhanced adiposity (Figures 1M and S2F). Numbers of early adipocyte progenitors in both visceral and subcutaneous fat of *mir-25-93-106b*$^{-/-}$ mice started to rise at 4 weeks of age and reached a maximum at 8 weeks (Figure S2G).

MiR-93 Inhibits Adipogenesis

To elucidate the roles of individual members of the *miR-25-93-106b* cluster in adipogenesis, we determined their expression in non-obese wild-type (WT) mice versus obese, leptin-deficient (*ob/ob*) mice. *MiR-93* and *miR-106b* were robustly expressed in many tissues of WT mice, including visceral and subcutaneous fat (Figure S3A). *MiR-93* was also significantly downregulated in visceral fat of *ob/ob* mice (Figure 2A; Table S1), suggesting a crucial role for miR-93 in visceral adipogenesis (Figure 2A). Indeed, inhibition of miR-93 strongly promoted in vitro adipocyte

Figure 1. Enhanced Adiposity and Adipogenesis in *miR-25-93-106b*$^{-/-}$ Mice

(A) Visceral fat (EWAT) in WT versus *miR-25-93-106b*$^{-/-}$ (KO) mice (top). Fat pads of white (EWAT) and brown (BAT) fat (bottom) are shown.

(B) Computed tomography in female WT and KO mice illustrates total body fat (n = 14; *p < 0.05; quantification [left] and representative images [right]).

(C) Separate analysis for SWAT and EWAT content is shown (n = 13; *p < 0.05; quantification [top] and representative images [bottom]).

(D) GTT in female WT and KO mice after injection of 2 g/kg BW glucose (n = 7; *p < 0.05) (left) and ITT in female WT and KO mice after injection of 1 IU/kg BW insulin (n = 7; *p < 0.05) (right) are shown.

(E) Insulin levels in blood plasma after 12 hr of fasting and 2 hr after re-feeding are shown (n = 8; *p < 0.05, **p < 0.05 versus WT).

(F) Indirect calorimetric measurements in WT versus KO mice. Energy expenditure (EE) was recorded for a period of two consecutive nights (gray shade).

(G) Mean EE in WT versus KO mice is shown (n = 8; *p < 0.05).

(H) Respiratory quotient in WT versus KO mice is shown (n = 8; n.s., not significant).

(I) Rearing activity in WT versus KO mice is shown (n = 8; *p < 0.05).

(J) Food intake in WT versus KO mice is shown (n = 8; *p = 0.09).

(K) Leptin in the blood plasma of KO and WT mice is shown (n = 16; *p < 0.05).

(L) Frequency distribution of the adipocyte area (size) in KO versus WT mice is shown (n $\geq$ 317 adipocytes; inset, representative images).

(M) Numbers of Lin^{-}CD24^{+}CD29^{+}SCA-1^{+}CD34^{+} early adipocyte precursors (APs) are shown (representative pictures, left; quantification, right [n = 4 mice; *p < 0.05]).

All data are presented as mean ± SEM. See also Figures S1 and S2.

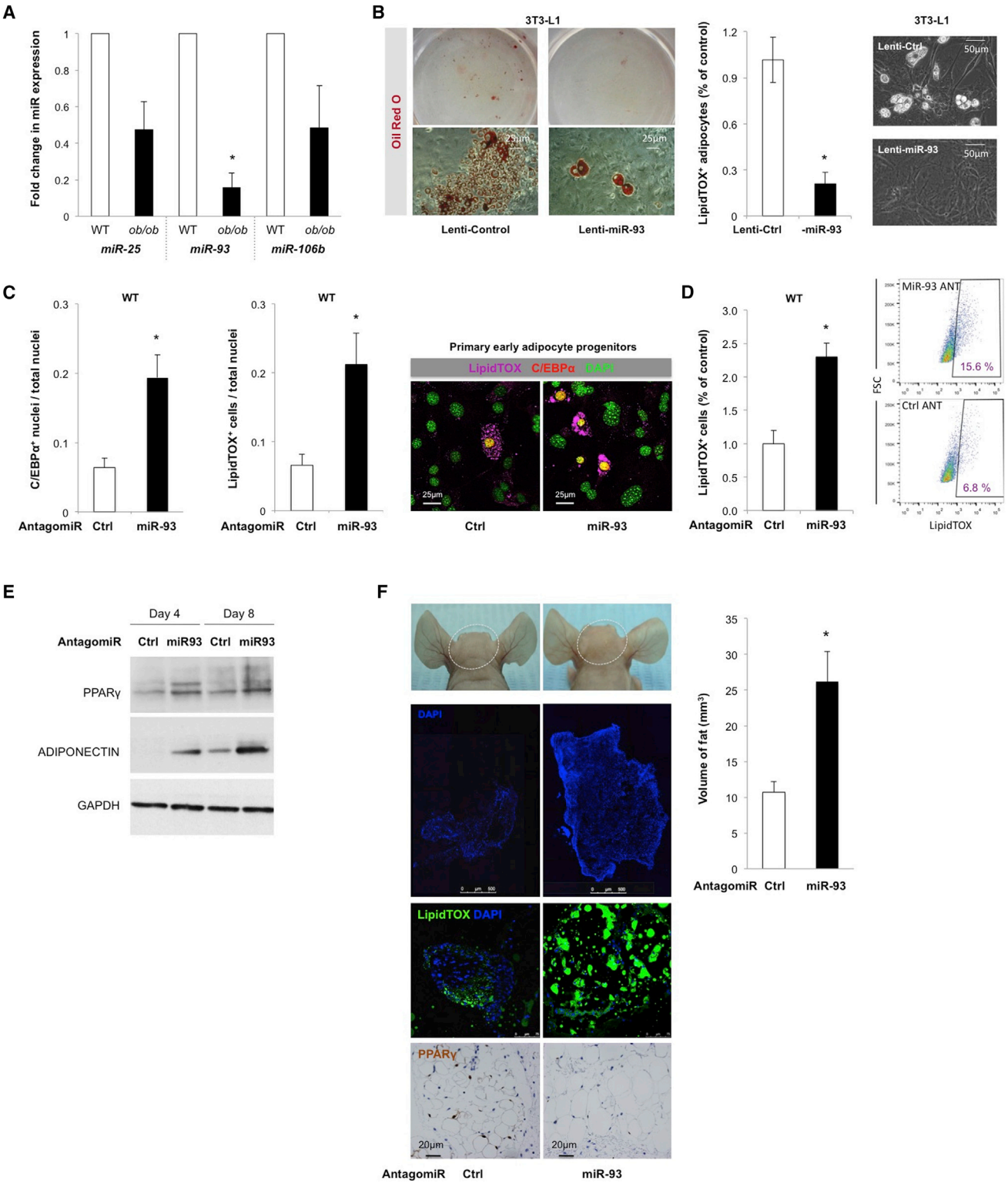

Figure 2. MiR-93 Inhibits Adipogenesis

(A) Expression of *miR-25*, *miR-93*, and *miR-106b* in total visceral fat of male obese *ob/ob* versus C57Bl/6J mice (28 weeks) is shown.

(B) 3T3-L1 pre-adipocytes transduced with control or *miR-93* lentiviral construct. Spontaneous differentiation was quantified by Oil Red O staining (left) or LipidTOX staining (middle) with representative images (right).

(legend continued on next page)

differentiation. In addition, miR-106b appeared to play a role in adipocyte differentiation (Figure S3B).

Given that miR-93 and miR-106b share putative target RNAs *Tbx3* and *Sirt7* (Figure S3C), we decided to focus on *miR-93*. Indeed, overexpression of *miR-93* repressed the normal spontaneous differentiation of 3T3-L1 pre-adipocytes into mature adipocytes (Figure 2B). In contrast, miR-93 antagomiR enhanced adipogenesis in WT early adipocyte precursors (Figures 2C–2E). We then tested whether miR-93 antagomiRs were capable of enhancing adipogenesis in vivo using freshly sorted early adipocyte precursor cells pretreated with miR-93 antagomiR. Occipital subcutaneous implantation of miR-93 antagomiR-treated early adipocyte progenitors produced larger adipose deposits relative to control-treated cells (Figures 2F, S3D, and S3E).

MiR-93 Counteracts Self-Renewal of Adipocyte Precursor via Tbx3

In silico prediction with http://www.microRNA.org identified numerous potential miR-93 targets. We focused on the transcription factor T-box 3 (*Tbx3*) based on its demonstrated role in maintaining pluripotency via regulation of *Nanog*, *Sox2*, *Oct4*, and *Klf4* (Han et al., 2010; Figure 3B). Indeed, *Tbx3* and the stemness genes *Nanog* and *Oct4* were consistently overexpressed in early adipocyte precursor cells and pre-adipocytes in WT mice, but levels in *mir-25-93-106b*$^{-/-}$ cells were further increased (Figures 3A–3C). In addition, *Tbx3* was expressed early during in vitro adipocyte differentiation (Figure S4A). Using 3′UTR constructs, we found that miR-93 mimics inhibit *Tbx3*-3′UTR-regulated luciferase activity, thereby confirming *Tbx3* as a target for miR-93 (Figure 3D).

To elucidate the functional role for *Tbx3* in early adipocyte precursors, we knocked down *Tbx3* in adipose tissue in mice kept on a 60% HFD to promote in vivo adipogenesis, which resulted in reduced numbers of early adipocyte precursors (Figure 3E). To corroborate these data, we ablated *Tbx3* in mature adipocytes using *adiponectin-Cre* (*Adi-Cre*;*Tbx3*$^{fl/fl}$), and we employed *PDGFRα-Cre* to eliminate *Tbx3* in early adipocyte precursors, pre-adipocytes, and mature adipocytes (*PDGFRα-Cre*;*Tbx3*$^{fl/fl}$, Figure 3F; Berry and Rodeheffer, 2013). Adult *Adi-Cre*;*Tbx3*$^{fl/fl}$ mice showed no adipose tissue-related phenotypes with the exception of a few females with slightly reduced gross adipose tissue and diminished CD31$^-$CD45$^-$CD24$^+$CD34$^+$SCA-1$^+$CD29$^+$ early adipocyte precursors (Figure S4B). Unfortunately, *PDGFRα-Cre*;*Tbx3*$^{fl/fl}$ mice were not viable postnatally, most likely due to a lethal cardiac phenotype (Frank et al., 2012). In WT mice at fetal stages E17.5-18.5, when adipocyte precursors, but not yet adipose tissue (Chau et al., 2014), are present, about 20% of CD31$^-$CD45$^-$CD24$^+$CD34$^+$CD29$^+$ cells in fresh fetal tissue were positive for the adipocyte precursor marker PDGFRα (Figure 3G). For *PDGFRα-Cre;Tbx3*$_{fl/fl}$ mice surviving to the same fetal stages, we observed a reduced number of PDGFRα$^+$ early adipocyte precursors, consistent with a crucial role for *Tbx3* in these cells.

To test whether loss of *Tbx3* prevents enhanced adipogenesis in response to miR-93 antagomiRs, PDGFRα$^+$ early adipocyte precursors were derived from first-passage mouse embryonic fibroblasts (MEFs), pretreated with miR-93 or control antagomiRs, and induced to differentiate into adipocytes (Rosen and MacDougald, 2006). While inhibition of *miR-93* resulted in higher numbers of lipid droplet$^+$ adipocytes in WT cells, this effect was absent in *Tbx3*$^{-/-}$ cells, which in contrast showed reduced lipid filling of adipocyte precursors (Figures 3H–3J). These results demonstrate that *Tbx3* is a functional downstream target of miR-93 and plays an important role in embryonic early adipocyte precursors and their differentiation into adipocytes.

MiR-93 Controls Adipogenesis via Sirt7

Although the mammalian *Sirtuin-7* (*Sirt7*) has a postulated role in adipogenesis (Shin et al., 2013), its physiological function remains largely unclear (Barber et al., 2012). *Sirt7* is another predicted target of miR-93 (Figure S3C) and is induced early during in vitro adipocyte differentiation (Figure S4A). As predicted, miR-93 inhibited *Sirt7* and adipogenesis (Figure 4A). Consistent with this, expression of *Sirt7* was enhanced in the stromal vascular fraction of visceral fat in *mir-25-93-106b*$^{-/-}$ (Figure 4B, left) and *ob/ob* mice (Figure 4B, middle), respectively, the latter correlating with decreased miR-93 levels in these mutants (Figure 2A). Moreover, 24-hr treatment of 3T3-L1 pre-adipocytes with miR-93 antagomiR caused upregulation of *Sirt7* (Figure 4B, right). *Sirt7* was overexpressed in early adipocyte precursor cells and pre-adipocytes in WT mice, but levels in *mir-25-93-106b*$^{-/-}$ mice were overall higher (Figure 4C). This was validated at the protein level using SIRT7 immunofluorescence (Figure 4D). On the other hand, gain-of-function experiments with miR-93 mimics injected into the visceral fat pads of *ob/ob* mice resulted in decreased nuclear SIRT7 immunoreactivity (Figure 4E).

To conclusively validate that miR-93 inhibits *Sirt7*, the *Sirt7*-3′UTR-Gaussia luciferase (Gluc) reporter was transduced into HEK293 cells, followed by transfection with miR-93 mimics. This led to marked suppression of luciferase activity (Figure 4E). Finally, the crucial role of *Sirt7* in adipogenesis was demonstrated directly by *Sirt7* knockdown, which resulted in reduced Oil Red O and adipocyte-lineage-marker staining for FABP4 (Figure 4F). Furthermore, expression of *Pparγ*, *C/ebpα*, and *Adipoq* was decreased in EWAT of *Sirt7*$^{-/-}$ mice (Figures 4H–4J). Early adipocyte precursors were reduced in *Sirt7*$^{-/-}$ mutants relative to controls (Figure 4K), as was expression of adipogenesis

(C) WT pre-adipocytes treated with antagomiR against control or *miR-93*. C/EBPα$^+$ cells (left) and LipidTOX$^+$ cells (middle) and representative confocal images (right) illustrate double staining for LipidTOX and C/EBPα.

(D) Quantification (left) and representative flow cytometry blots (right) for LipidTOX lipid staining are shown (n = 4; $p < 0.05$).

(E) Western blot analysis for protein expression of PPARγ and adiponectin in WT pre-adipocytes treated with antagomiR against control or *miR-93*. GAPDH was used as a loading control.

(F) In vivo adipogenesis at the occipital skull region of nude mice (circled by hash-line, first row). DAPI (second row) and LipidTOX (third row) staining of explanted fat tissue; immunostaining for PPARγ to detect cells of adipocyte lineage (fourth row); and quantification of the volume (right) are shown (n = 6; *$p < 0.05$).

All data are presented as mean ± SEM. See also Figure S3.

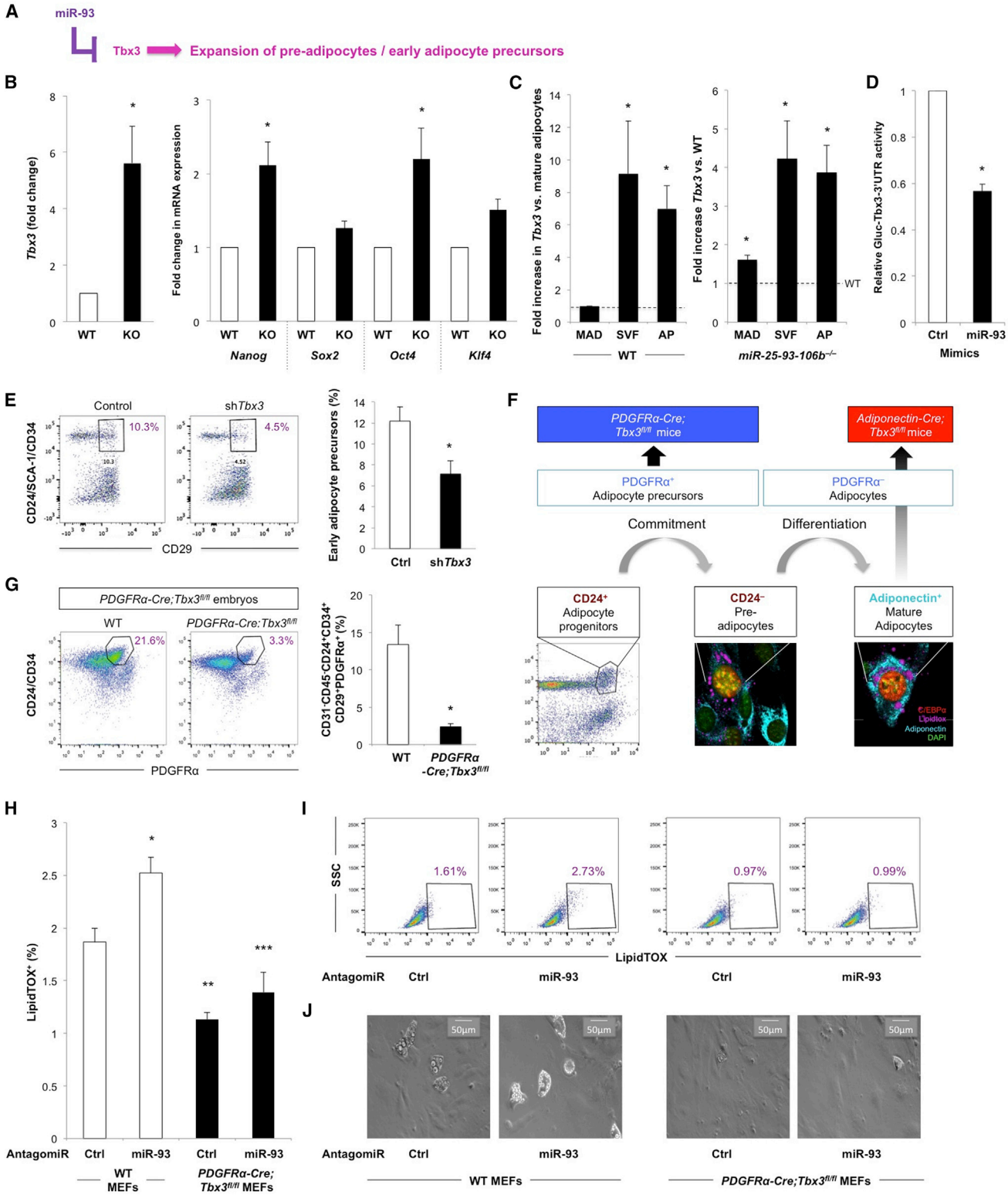

Figure 3. miR-93 Counteracts Self-Renewal of Adipocyte Precursors via Tbx3

(A) *MiR-93* inhibits expansion of early APs and pre-adipocytes via inhibition of Tbx-3.

(B) (Left) Relative expression of *Tbx3* in early APs was measured by quantitative real-time PCR (n = 3; *p < 0.05). (Right) Relative expression of pluripotency-associated genes in early APs was measured by quantitative real-time PCR (n = 3; *p < 0.05).

(legend continued on next page)

markers in response to in vitro adipocyte differentiation (Figures 4L and 4M). Finally, the increase in lipid droplet$^+$ cells observed in response to miR-93 antagomiR treatment was diminished in *Sirt7*$^{-/-}$ mice, demonstrating that *Sirt7* is a functionally relevant miR-93 target (Figure 4N).

Circulating Endogenous Factors or Local Injection of miR-93 Reduces Size of Visceral Fat Pads

Circulating adiponectin levels were higher in WT females compared to WT males (Luque-Ramírez et al., 2013) and reduced in female *mir-25-93-106b*$^{-/-}$ mice (Figure 5A), confirming the endocrine function of visceral adipose tissue. Intriguingly, adiponectin levels in *mir-25-93-106b*$^{-/-}$ mice could be rescued by transplantation with WT bone marrow cells (Figure 5B). This reveals that adiponectin is not a direct target of miR-93, but rather an indirect factor modulated in response to the metabolic abnormalities in these mutants. This predicts that systemic delivery of the miR-25-93-106b cluster or miR-93 should reduce visceral fat burden. Non-obese WT females had a higher circulating miR-93 level compared to WT males, while *mir-25-93-106b*$^{-/-}$ mice did not have detectable miR-93 levels and served as a negative control (Figures 5C and S5A). Consistent with the notion that *miR-93* expression is estrogen dependent, miR-93 levels increased during pregnancy and decreased after ovarectomy (Figure S5B). To validate that circulating miR-93 is functionally active and capable of inhibiting *Sirt7*, HEK293 cells expressing the *Sirt7*-3′ UTR-Gaussia luciferase reporter were exposed to either 20% WT or *mir-25-93-106b*$^{-/-}$ plasma; WT plasma reduced reporter activity by 50%, but there was no response to KO plasma (Figure 5D).

To investigate whether circulating miRNA can rescue *mir-25-93-106b*$^{-/-}$ phenotypes and reduce visceral fat, we created parabiotic pairs from female WT and *mir-25-93-106b*$^{-/-}$ mice (Figure 5E). After 8 weeks, we observed reduced visceral and subcutaneous fat in *mir-25-93-106b*$^{-/-}$ mice (Figures 5F and 5G), accompanied by reduced levels of *Sirt7* and *Tbx3* (Figure 5H) and normalization of adiponectin and leptin plasma levels (Figures S5C–S5F). We tested the therapeutic effect of restoring miR-93 levels by locally injecting liposomal miR-93 into the visceral fat of *ob/ob* mice (Figure S5G), which resulted in reduced visceral fat after 4 weeks (Figure 5I). Strikingly, glucose tolerance had already improved at this point, confirming the strong metabolic impact of miR-93 (Figure 5J). Finally, we aimed at reversing the obese phenotype in female *mir-25-93-106b*$^{-/-}$ mice (Figure 5K). We reconstituted miR-93 into *mir-25-93-106b*$^{-/-}$ bone marrow-derived stromal cells (Figure 5L), and we injected reconstituted or control cells into the perineal adipose tissue. After 12 weeks, flow cytometry revealed reduced numbers of early adipocyte precursor cells (Figure 5M) and PPARγ^+ cells (Figure 5N) in the perineal tissue of mice treated with miR-93-reconstituted cells, indicating successful reversal of adiposity.

DISCUSSION

Mir-25-93-106b$^{-/-}$ mice have increased intra-abdominal, perineal, and subcutaneous fat and subsequent increased insulin resistance. Consistent with this, obese *ob/ob* mice have significant downregulation of *miR-93* (Ventura et al., 2008) and *miR-93* also is downregulated in hyperglycemia (Long et al., 2010). Thus, our data suggest a vicious cycle in which pre-diabetic conditions characterized by impaired glucose tolerance and insulin resistance lead to reduced miR-93 levels that in turn accelerate adipogenesis, worsening the diabetic condition and leading to further suppression of miR-93. Mechanistically, we show that suppression of miR-93 augments white adipose tissue by increasing adipocyte precursors through the pluripotency-associated transcription factor *Tbx3* and by increasing adipogenesis through *Sirt7*. Restoring miR-93 by either systemic delivery in a parabiosis model or direct injection into the visceral fat pads reduced fat mass and improved insulin sensitivity. These data demonstrate that miR-93 serves as an important regulator for in vivo visceral white fat adipogenesis.

Increased fat mass in obesity is currently attributed to two mechanisms: adipocyte hypertrophy, in which pre-existing adipocytes increase their size due to lipid accumulation; and adipocyte hyperplasia, leading to increased numbers of adipocytes by differentiation of pre-adipocytes. New adipocytes in vivo are derived from progenitors that recently have been described as early adipocyte progenitor cells and are defined as Lin-CD24$^+$CD29$^+$CD34$^+$SCA-1$^+$ cells resident in the adult white adipose tissue vascular stroma (Berry and Rodeheffer, 2013; Rodeheffer et al., 2008). Here we show that these early adipocyte progenitors are increased in the enhanced abdominal and

(C) Expression of *Tbx3* (left) in mature adipocytes (MADs), stromal-vascular pre-adipocytes (SVFs), and early APs. Baseline levels are given in the first bar indicating MADs and by the dotted line (n = 4; *p < 0.05 versus MADs, right). Expression of *Tbx3* in MADs, SVFs, and early APs in *miR-25-93-106b*$^{-/-}$ versus WT mice is shown. Baseline levels of WT mice are indicated by the dotted line (n = 4; *p < 0.05 for *miR-25-93-106b*$^{-/-}$ versus WT).

(D) 3′UTR-*Tbx3* Gaussia luciferase activity in HEK293 in the presence or absence of miR-93 mimics is shown (n = 3, *p < 0.05 for *miR-93* mimic versus Ctrl).

(E) Injection of lentiviral sh*Tbx3* into the adipose tissue of *miR-25-93-106b*$^{-/-}$ mice, followed by flow cytometric analysis of early APs is shown by representative pictures (left) and quantification (right) (n = 3; *p < 0.05).

(F) Scheme indicating MADs as targets of adiponectin and APs as targets of PDGFRα. The generation of *Adiponectin-Cre*;*Tbx3*$^{fl/fl}$ and *PDGFRα-Cre*;*Tbx3*$^{fl/fl}$ mice to ablate *Tbx3* in MADs and APs, respectively, is shown.

(G) Flow cytometry of early APs from fetuses (E17.5–18.5) of *PDGFRα-Cre*;*Tbx3*$^{fl/fl}$ mice versus controls (n = 5; *p < 0.05). Representative flow cytometry of early APs (left) is shown and quantified (right).

(H) Early APs from *PDGFRα-Cre*;*Tbx3*$^{fl/fl}$ mice versus controls were sorted for expression of early AP markers, including expression of PDGFRα, cultured, and at confluency differentiated into adipocytes for 4 days in the presence or absence of miR-93 or control antagomiRs. LipidTOX$^+$ lipid-droplet-containing cells were analyzed (n = 4; *p < 0.05 for WT + miR-93-ANT versus WT + ctrl-ANT, **p < 0.05 for *Tbx3* mutant + ctrl-ANT versus WT + ctrl-ANT, ***p < 0.05 for *Tbx3* mutant + miR-93-ANT versus WT + miR-93-ANT).

(I and J) Representative flow cytometry (I) and images of the lipid-droplet-containing cells (J) are displayed.

All data are presented as mean ± SEM. See also Figure S4.

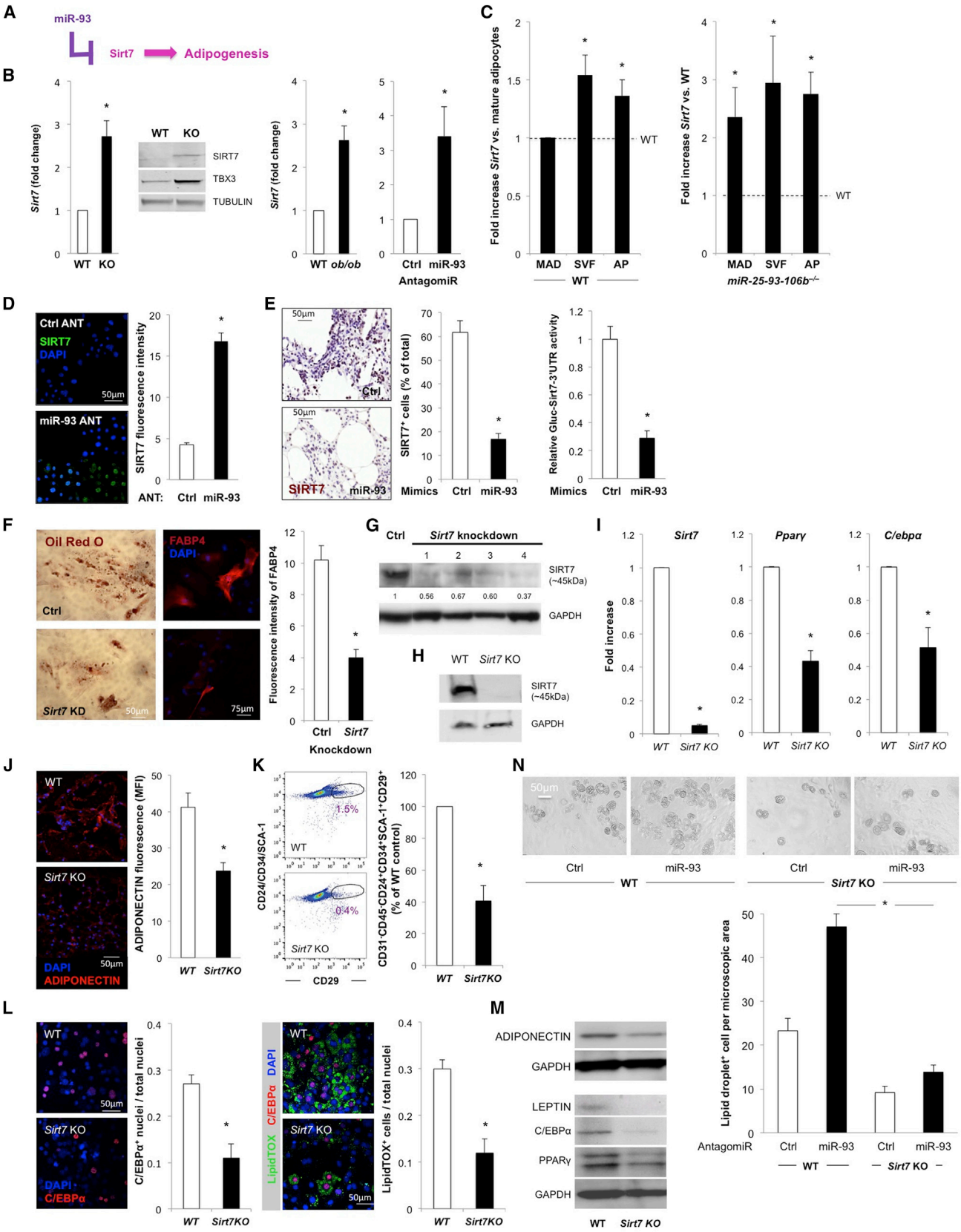

(legend on next page)

subcutaneous fat of *mir-25-93-106b*$^{-/-}$ mice, suggesting that increased fat mass is not merely related to adipocyte hyperplasia, but to enhanced generation of new adipocytes. Intriguingly, this difference was only observed in younger mice (8 weeks), while older mice (18 weeks) showed a sharp drop in the number of early adipocyte progenitors, so that no later differences could be observed between WT and *mir-25-93-106b*$^{-/-}$ mice. Moreover, we demonstrated that metabolic changes, such as reduced EE due to low rearing activity, contribute to increased fat mass. However, we cannot discriminate whether these metabolic disturbances are the cause or consequence of some or all of the *mir-25-93-106b*$^{-/-}$ phenotypes. Our data support the postulate that early progenitor cells predominantly play a role in obesity during adolescence and early adulthood, while adipogenesis is mostly driven by adipocyte hyperplasia later in life.

Adipose tissue is not a quiescent organ: rapid turnover of the adipocyte population has been described (Rigamonti et al., 2011). About 5% of pre-adipocytes are replicating at any time and 1%–5% of adipocytes are replaced each day. This process appears to be tightly controlled by miR-93. Our observation that pretreatment with miR-93 antagomiR increases formation of adipocyte tissue in vivo validates the inhibitory role of miR-93 on in vivo functionality of early adipocyte precursors. Together with the excess expansion of the pool of early adipocyte progenitor in *mir-25-93-106b*$^{-/-}$ mice, our data suggest enhanced self-renewal as the driving mechanism.

Several miRNAs are key regulators of stem cell maintenance and promotion of differentiation (Gangaraju and Lin, 2009). For example, miR-302 and miR-290 regulate self-renewal in embryonic stem cells (Le Bot, 2012). Notably, the role of miRNAs for self-renewal in early adipocyte precursors had not been described previously. In our search for putative stem cell-related targets that might explain the expansion of the early adipocyte precursor pool following suppression of miR-93, we identified the transcription factor *Tbx3* as a candidate. Indeed, Tbx3 promotes mesendodermal differentiation during embryogenesis (Weidgang et al., 2013). Our data from fetuses in which *Tbx3* was ablated in PDGFR cells support this notion and demonstrate a key role for Tbx3 in early adipocyte precursors. In pluripotent stem cells, Tbx3 maintains pluripotency, promotes self-renewal, and facilitates reprogramming by direct binding of the *Oct4* promoter (Han et al., 2010). Consistent with this, a diabetic microenvironment enhances *Oct4* and *Nanog* expression in human visceral-derived adipose stem cells (Dentelli et al., 2013). *Tbx3* overexpression also causes mammary gland hyperplasia and increases mammary stem-like cells in an inducible transgenic mouse model (Liu et al., 2011). Here we show that Tbx3 and downstream transcriptional regulators of the pluripotency network, such as *Nanog* and *Oct4*, also are increased in early adipocyte progenitor cells of *mir-25-93-106b*$^{-/-}$ mice compared to WT littermates. However, our study does not distinguish whether it is these pluripotency-associated factors or other unknown regulators that maintain cells in the precursor state or promote adipocyte lineage commitment. As functional proof of its role in the self-renewal capacity of early adipocyte precursors, we found that knockdown and knockout (KO) of *Tbx3* reduced the number of adipocyte precursors in vivo. Also, we showed that *Tbx3* is a direct target of miR-93 in vitro.

In addition to enhanced early adipocyte progenitor activity, increased fat mass in *mir-25-93-106b*$^{-/-}$ mice may be related to increased adipogenesis with lipid accumulation in pre-existing or newly formed adipocytes. Indeed, we provide evidence for this second mechanism of action. Following expansion of early adipocyte precursors via *Tbx3* during early adolescence, subsequent Sirt7 activity (another predicted target of miR-93) drives adipogenesis. This eventually materializes as increased fat

Figure 4. MiR-93 Controls Adipogenesis via Sirt7

(A) MiR-93 inhibits pro-adipogenic Sirt7.

(B) *Sirt7* mRNA (and protein in inset) expression in WT versus *mir-25-93-106b*$^{-/-}$ (KO) mice (n = 5; *p < 0.05, western blot left), WT versus *ob/ob* leptin-deficient mice (n = 3; *p < 0.05, middle), and expression of *Sirt7* in the presence of miR-93 and control antagomiR in 3T3-L1 after 3 days of adipocyte differentiation by real-time qPCR (n = 3; *p < 0.05, right) are shown.

(C) Expression of *Sirt7* (left) in MADs, SVFs, and early APs. Baseline levels are given in the first bar indicating MADs and by the dotted line (n = 4; *p < 0.05 versus MADs). (Right) Expression of *Sirt7* in MADs, SVFs, and early APs in *miR-25-93-106b*$^{-/-}$ versus WT mice is shown. Baseline levels of WT mice are indicated by the dotted line (n = 4; *p < 0.05 for *miR-25-93-106b*$^{-/-}$ versus WT).

(D) Quantification of *Sirt7* immunofluorescence (green) in the presence of miR-93 and control antagomiR in 3T3-L1 cells after 24 hr of adipocyte differentiation (right) and representative images (left) are shown.

(E) Immunohistochemistry for SIRT7 in WT versus *ob/ob* mice following treatment with miR-93 mimics (left), quantification of SIRT^{+} cells (middle), and *Sirt7-3′UTR*-Gaussia luciferase activity in HEK293 in the presence or absence of miR-93 mimics (right) are shown (n = 4; *p < 0.05).

(F–I) Oil Red O staining (left), FABP4 immunostaining (middle), and quantification of FABP4 staining (n = 7; *p < 0.05, right) in human adipose tissue-derived pre-adipocytes following *Sirt7* knockdown (F) as demonstrated by western blot for SIRT7 (G). Lack of SIRT7 protein expression (H) and mRNA expression (I, left) in EWAT of *Sirt7* KO versus WT mice is shown. *Pparγ* (I, middle) and *C/ebpα* (I, right) mRNA expression in EWAT tissue of *Sirt7* KO versus WT mice is shown (n = 3; *p < 0.05).

(J) Adiponectin immunostaining in frozen sections from EWAT of *Sirt7* KO versus WT mice is depicted in representative images (left) and quantitative analysis (right; n = 4–5; *p < 0.05).

(K) Flow cytometry of early APs in *Sirt7* KO versus WT. Representative images (left) and quantification (right) are shown (n = 4; *p < 0.05).

(L) In vitro fat differentiation of *Sirt7* KO and WT-derived sorted early APs. Confocal microscopy analysis shows nuclear C/EBPα immunostaining (left) and analysis of lipid droplets (right) identified by the lipid stain LipidTOX (DAPI is nuclear stain). Quantification and representative pictures are exhibited (n = 7; *p < 0.05).

(M) Protein expression of adiponectin (day 8 of fat differentiation) and leptin, C/EBPα, and PPARγ (day 4) in *Sirt7* KO versus WT-derived early APs. GAPDH was the loading control.

(N) In vitro fat differentiation of *Sirt7* KO and WT-derived sorted early APs for 8 days in the presence of miR-93 or control antagomiR. Quantification (bottom) and representative pictures (top) are displayed (n = 6; *p < 0.05).

All data are presented as mean ± SEM. See also Figure S4.

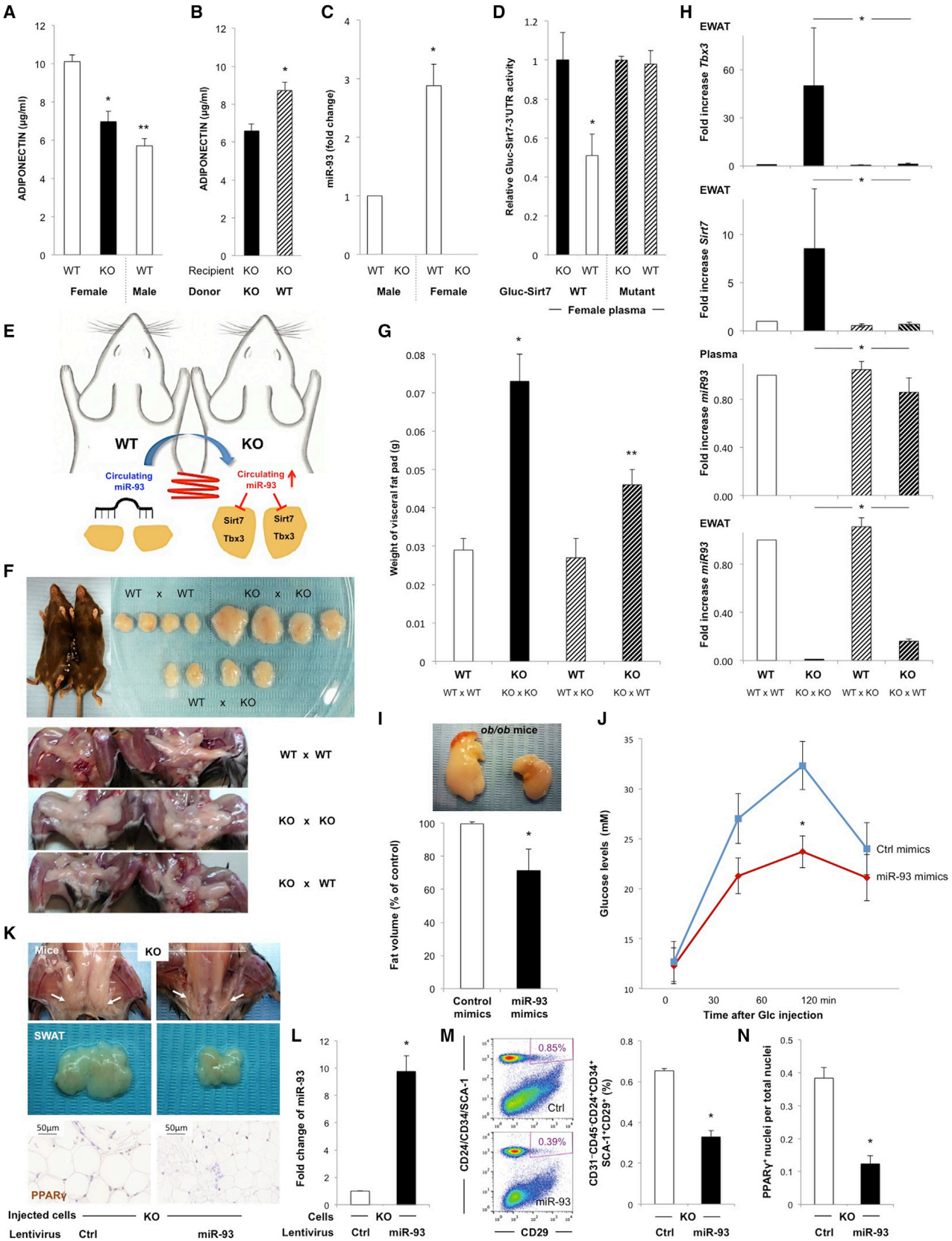

(legend on next page)

mass in adulthood. The *Sirtuin* family of nicotinamide adenine dinucleotide (NAD^+)-dependent deacetylases has a well-established role in energy metabolism. However, the role of the more recently described family member *Sirt7* in metabolic regulation has not yet been well defined. Mechanistically, Sirt7 specifically deacetylates histone H3 lysine 18 (H3K18) and promotes transcriptional repression (Barber et al., 2012). Although it was reported that *Sirt7*$^{-/-}$ mice have less visceral fat (Shin et al., 2013), the regulation of adipogenesis by Sirt7 had not been fully explored. We now provide conclusive evidence that Sirt7 is a direct target of miR-93 and regulates the *Sirt7*-3′UTR-Gaussia luciferase reporter. Following *Sirt7* knockdown in vitro and *Sirt7* KO in vivo, adipogenesis in vitro and adiposity in vivo were both clearly reduced and demonstrate a role for *Sirt7* in promoting obesity.

The metabolic and health consequences of increased fat mass, especially visceral fat, are serious: insulin resistance and adipocyte dysfunction. Therefore, inhibition of adipogenesis via upregulation of *miR-93* plays a crucial role in attenuating metabolic disorders and, subsequently, ameliorating the increased cardiovascular risk. Intriguingly, we provide two lines of evidence that enhancing miR-93 levels indeed reduces fat volume and mass as well as secondary metabolic alterations. First, we used a parabiosis model to systemically deliver WT miRNA to *mir-25-93-106b*$^{-/-}$ mice via cross-circulation that is spontaneously established between the two parabionts, and we demonstrated that levels of miR-93 are indeed reconstituted in the parabiotic *mir-25-93-106b*$^{-/-}$ partner. However, levels of non-miR-93 targets, such as adiponectin and leptin, also were normalized and we cannot preclude their contribution to the reversal of the fat phenotype in parabiotic partners. Second, we injected miR-93 directly into the intra-abdominal fat pads of *ob/ob* mice. Both approaches resulted in a similarly improved phenotype, demonstrating that miR-93 is crucial and a tractable therapeutic intervention for inhibiting excessive adipogenesis. However, when considering miR-93 mimics as potential therapeutic agents to conquer obesity, we must consider that *miR-93* frequently is overexpressed in human cancer and has been reported to promote tumor growth (Fang et al., 2011). Indeed, cancer-induced cachexia might be further enhanced or even initiated by tumors overexpressing *miR-93*. Paradoxically, however, miR-93 also has been found to function as a tumor suppressor in some contexts (Liu et al., 2012). Therefore, additional studies are needed to fully understand the role of miR-93 in cancer.

EXPERIMENTAL PROCEDURES

Animal Studies

Studies were performed with miR-25-93-106b$^{-/-}$ mice and their littermates on C57BL/6J background (a kind gift of Andrea Ventura) and *ob/ob* mice from The Jackson Laboratory. Parabiotic couples of female WT and *mir-25-93-106b*$^{-/-}$ mice were created as previously published (Aicher et al., 2007). All animal studies were approved by the Institute's Institutional Animal Care and Use Committee (CBA 26_2009, CBA 25_2009, CBA 68_2013, and PPL70-8129).

Glucose Measurements

To perform the glucose tolerance test (GTT) and insulin tolerance test (ITT), fasting glucose was measured in mice after a 12-hr fast. Blood samples to obtain serum were drawn retroorbitally. For the GTT, mice were intraperitoneally injected with 2 g/kg BW glucose (Sigma-Aldrich). For the ITT, 1 IU/kg BW insulin (Sigma-Aldrich) was intraperitoneally injected. To measure serum glucose, blood samples were drawn at 30, 60, and 120 min post-injection. Serum glucose (in mmol/l) was determined using an ABX Pentra 400 clinical chemistry analyzer (Horiba ABX Diagnostics).

SUPPLEMENTAL INFORMATION

Supplemental Information includes Supplemental Experimental Procedures, five figures, and one table and can be found with this article online at http://dx.doi.org/10.1016/j.celrep.2015.08.006.

AUTHOR CONTRIBUTIONS

M.C., M.V.S., S.M.T., A.N.F., C.R.V., B.G.G., A.C.-G., V.H., J.A.C., F.M., U.P.C., M.P., J.S., D.M., D.R., and P.J.F.-M. conducted and analyzed experiments. S.H. designed, conducted, and analyzed the miRNA microarrays. B.N.V. and L.S. provided Sirt7 KO mice and edited the manuscript. A.M. generated Tbx3 mutant mice, analyzed data, and edited the paper. A.A. and C.H. conceived the study, wrote the paper, designed the experiments, and analyzed and interpreted data.

ACKNOWLEDGMENTS

We graciously thank Flor Diaz for expert technical assistance. We are grateful to Andrea Ventura for providing the *mir-25-93-106b*$^{-/-}$ mice and Elena

Figure 5. Circulating Endogenous Factors or Local Injection of miR-93 Reduces Visceral Fat Pads

(A) Adiponectin plasma levels in WT versus *mir-25-93-106b*$^{-/-}$ (KO) mice are shown (n = 6; *p < 0.05).

(B) Adiponectin plasma levels in female KO mice following transplantation with WT or KO bone marrow are shown (n = 6; *p < 0.05).

(C) Levels of miR-93 in peripheral blood plasma of female and male WT and miR-25-93-106b cluster KO mice are shown (n = 4; *p < 0.05).

(D) *Sirt7*-3′UTR and mutated *Sirt7-3′UTR* luciferase activity in HEK293 in the presence of miR-93-containing female WT plasma or KO plasma is shown (n = 7–9; *p < 0.05).

(E) Schematic illustrates the parabiosis experiments.

(F) Representative visceral fat pads from parabiotic pairs 8 weeks after surgical joining (top) and subcutaneous fat in the perineal region (bottom) are shown.

(G) Quantification of (F) is shown (n = 6–8 visceral fat pads; *p < 0.05).

(H) mRNA expression of *Tbx3* and *Sirt7* in EWAT as well as miR93 levels in plasma and EWAT, respectively, of parabiotic mice are shown (n ≥ 4; *p < 0.05).

(I) Visceral fat pads of male obese *ob/ob* mice 4 weeks after local injection of miR-93 mimics versus control (top) and quantification (bottom) are shown (n = 3; *p < 0.05).

(J) GTT in obese *ob/ob* mice following treatment with miR-93 mimics versus control (n = 3; *p < 0.05).

(K and L) In vivo reversal of the obese phenotype of female KO mice. Injection of KO MSCs with or without lentiviral *miR-93* overexpression (L) into the subcutaneous perineal region (arrows) is shown. Gross morphology in situ (K, top) and after explantation of subcutaneous adipose tissue (middle), followed by histological analysis (bottom) is shown.

(M) Flow cytometry of early AP in reversed (bottom, *miR-93*) adipose tissue relative to control (top, Ctrl) is shown (n = 3; *p < 0.05).

(N) Quantification of PPARγ^+ adipocytes is shown (n = 3; *p < 0.05).

All data are presented as mean ± SEM. See also Figure S5.

Lopez-Guadamillas for providing visceral fad pads from *ob/ob* mice. Research was supported by the European Research Council Advanced Investigator Grant (Pa-CSC 233460) and the European Community's Seventh Framework Programme (FP7/2007-2013) under grant agreements 256974 (EPC-TM-NET) and 602783 (CAM-PaC). M.C. was supported by a La Caixa Fellowship.

Received: June 11, 2015
Revised: July 24, 2015
Accepted: August 2, 2015
Published: August 27, 2015

REFERENCES

Aicher, A., Rentsch, M., Sasaki, K., Ellwart, J.W., Fändrich, F., Siebert, R., Cooke, J.P., Dimmeler, S., and Heeschen, C. (2007). Nonbone marrow-derived circulating progenitor cells contribute to postnatal neovascularization following tissue ischemia. Circ. Res. *100*, 581–589.

Barber, M.F., Michishita-Kioi, E., Xi, Y., Tasselli, L., Kioi, M., Moqtaderi, Z., Tennen, R.I., Paredes, S., Young, N.L., Chen, K., et al. (2012). SIRT7 links H3K18 deacetylation to maintenance of oncogenic transformation. Nature *487*, 114–118.

Berry, R., and Rodeheffer, M.S. (2013). Characterization of the adipocyte cellular lineage in vivo. Nat. Cell Biol. *15*, 302–308.

Berry, R., Jeffery, E., and Rodeheffer, M.S. (2014). Weighing in on adipocyte precursors. Cell Metab. *19*, 8–20.

Chau, Y.Y., Bandiera, R., Serrels, A., Martínez-Estrada, O.M., Qing, W., Lee, M., Slight, J., Thornburn, A., Berry, R., McHaffie, S., et al. (2014). Visceral and subcutaneous fat have different origins and evidence supports a mesothelial source. Nat. Cell Biol. *16*, 367–375.

Chen, Y.H., Heneidi, S., Lee, J.M., Layman, L.C., Stepp, D.W., Gamboa, G.M., Chen, B.S., Chazenbalk, G., and Azziz, R. (2013). miRNA-93 inhibits GLUT4 and is overexpressed in adipose tissue of polycystic ovary syndrome patients and women with insulin resistance. Diabetes *62*, 2278–2286.

Dentelli, P., Barale, C., Togliatto, G., Trombetta, A., Olgasi, C., Gili, M., Riganti, C., Toppino, M., and Brizzi, M.F. (2013). A diabetic milieu promotes OCT4 and NANOG production in human visceral-derived adipose stem cells. Diabetologia *56*, 173–184.

Fang, L., Deng, Z., Shatseva, T., Yang, J., Peng, C., Du, W.W., Yee, A.J., Ang, L.C., He, C., Shan, S.W., and Yang, B.B. (2011). MicroRNA miR-93 promotes tumor growth and angiogenesis by targeting integrin-β8. Oncogene *30*, 806–821.

Frank, D.U., Carter, K.L., Thomas, K.R., Burr, R.M., Bakker, M.L., Coetzee, W.A., Tristani-Firouzi, M., Bamshad, M.J., Christoffels, V.M., and Moon, A.M. (2012). Lethal arrhythmias in Tbx3-deficient mice reveal extreme dosage sensitivity of cardiac conduction system function and homeostasis. Proc. Natl. Acad. Sci. USA *109*, E154–E163.

Gangaraju, V.K., and Lin, H. (2009). MicroRNAs: key regulators of stem cells. Nat. Rev. Mol. Cell Biol. *10*, 116–125.

Hamdy, O., Porramatikul, S., and Al-Ozairi, E. (2006). Metabolic obesity: the paradox between visceral and subcutaneous fat. Curr. Diabetes Rev. *2*, 367–373.

Han, J., Yuan, P., Yang, H., Zhang, J., Soh, B.S., Li, P., Lim, S.L., Cao, S., Tay, J., Orlov, Y.L., et al. (2010). Tbx3 improves the germ-line competency of induced pluripotent stem cells. Nature *463*, 1096–1100.

Klein, S., Allison, D.B., Heymsfield, S.B., Kelley, D.E., Leibel, R.L., Nonas, C., and Kahn, R. (2007). Waist Circumference and Cardiometabolic Risk: a Consensus Statement from Shaping America's Health: Association for Weight Management and Obesity Prevention; NAASO, the Obesity Society; the American Society for Nutrition; and the American Diabetes Association. Obesity (Silver Spring) *15*, 1061–1067.

Le Bot, N. (2012). miRNAs and cell-cycle control in ESCs. Nat. Cell Biol. *14*, 658.

Leyva, F., Godsland, I.F., Ghatei, M., Proudler, A.J., Aldis, S., Walton, C., Bloom, S., and Stevenson, J.C. (1998). Hyperleptinemia as a component of a metabolic syndrome of cardiovascular risk. Arterioscler. Thromb. Vasc. Biol. *18*, 928–933.

Liu, J., Esmailpour, T., Shang, X., Gulsen, G., Liu, A., and Huang, T. (2011). TBX3 over-expression causes mammary gland hyperplasia and increases mammary stem-like cells in an inducible transgenic mouse model. BMC Dev. Biol. *11*, 65.

Liu, S., Patel, S.H., Ginestier, C., Ibarra, I., Martin-Trevino, R., Bai, S., McDermott, S.P., Shang, L., Ke, J., Ou, S.J., et al. (2012). MicroRNA93 regulates proliferation and differentiation of normal and malignant breast stem cells. PLoS Genet. *8*, e1002751.

Long, J., Wang, Y., Wang, W., Chang, B.H., and Danesh, F.R. (2010). Identification of microRNA-93 as a novel regulator of vascular endothelial growth factor in hyperglycemic conditions. J. Biol. Chem. *285*, 23457–23465.

Luque-Ramírez, M., Martínez-García, M.A., Montes-Nieto, R., Fernández-Durán, E., Insenser, M., Alpañés, M., and Escobar-Morreale, H.F. (2013). Sexual dimorphism in adipose tissue function as evidenced by circulating adipokine concentrations in the fasting state and after an oral glucose challenge. Hum. Reprod. *28*, 1908–1918.

Nanayakkara, G., Kariharan, T., Wang, L., Zhong, J., and Amin, R. (2012). The cardio-protective signaling and mechanisms of adiponectin. Am. J. Cardiovasc. Dis. *2*, 253–266.

Phillips, R.J., Burdick, M.D., Hong, K., Lutz, M.A., Murray, L.A., Xue, Y.Y., Belperio, J.A., Keane, M.P., and Strieter, R.M. (2004). Circulating fibrocytes traffic to the lungs in response to CXCL12 and mediate fibrosis. J. Clin. Invest. *114*, 438–446.

Rigamonti, A., Brennand, K., Lau, F., and Cowan, C.A. (2011). Rapid cellular turnover in adipose tissue. PLoS ONE *6*, e17637.

Rodeheffer, M.S., Birsoy, K., and Friedman, J.M. (2008). Identification of white adipocyte progenitor cells in vivo. Cell *135*, 240–249.

Rosen, E.D., and MacDougald, O.A. (2006). Adipocyte differentiation from the inside out. Nat. Rev. Mol. Cell Biol. *7*, 885–896.

Shin, J., He, M., Liu, Y., Paredes, S., Villanova, L., Brown, K., Qiu, X., Nabavi, N., Mohrin, M., Wojnoonski, K., et al. (2013). SIRT7 represses Myc activity to suppress ER stress and prevent fatty liver disease. Cell Rep. *5*, 654–665.

Ventura, A., Young, A.G., Winslow, M.M., Lintault, L., Meissner, A., Erkeland, S.J., Newman, J., Bronson, R.T., Crowley, D., Stone, J.R., et al. (2008). Targeted deletion reveals essential and overlapping functions of the miR-17 through 92 family of miRNA clusters. Cell *132*, 875–886.

Wang, Q., Li, Y.C., Wang, J., Kong, J., Qi, Y., Quigg, R.J., and Li, X. (2008). miR-17-92 cluster accelerates adipocyte differentiation by negatively regulating tumor-suppressor Rb2/p130. Proc. Natl. Acad. Sci. USA *105*, 2889–2894.

Weidgang, C.E., Russell, R., Tata, P.R., Kühl, S.J., Illing, A., Müller, M., Lin, Q., Brunner, C., Boeckers, T.M., Bauer, K., et al. (2013). TBX3 Directs Cell-Fate Decision toward Mesendoderm. Stem Cell Reports *1*, 248–265.

Wentworth, J.M., Naselli, G., Brown, W.A., Doyle, L., Phipson, B., Smyth, G.K., Wabitsch, M., O'Brien, P.E., and Harrison, L.C. (2010). Pro-inflammatory CD11c+CD206+ adipose tissue macrophages are associated with insulin resistance in human obesity. Diabetes *59*, 1648–1656.

Wu, Y., Zuo, J., Zhang, Y., Xie, Y., Hu, F., Chen, L., Liu, B., and Liu, F. (2013). Identification of miR-106b-93 as a negative regulator of brown adipocyte differentiation. Biochem. Biophys. Res. Commun. *438*, 575–580.